ELSEVIER

Journal of Molecular Catalysis A: Chemical 162 (2000) 159–174

JOURNAL OF MOLECULAR CATALYSIS A: CHEMICAL

www.elsevier.com/locate/molcata

# Identification of active sites and adsorption complexes in Fe/MFI catalysts for $NO_x$ reduction

H.-Y. Chen [a], El-M. El-Malki [a], X. Wang [a], R.A. van Santen [b], W.M.H. Sachtler [a,*]

[a] *V.N. Ipatieff Laboratory, Center for Catalysis and Surface Science, Department of Chemistry, Northwestern University, Evanston, IL 60208, USA*

[b] *Schuit Institute of Catalysis, Eindhoven University of Technology, P.O. Box 513, 3600MB, Netherlands*

**Abstract**

FTIR, extended X-ray absorption fine structure (EXAFS) and X-ray absorption near edge spectroscopy (XANES) and ESR were used to identify the active sites and the adsorption complexes present in a variety of Fe/MFI samples prepared in different ways and displaying vastly different activities and selectivities in the reduction of $NO_x$ to $N_2$ with hydrocarbons. Iron oxide particles, charged ferric oxide nano-clusters, isolated iron ions and oxygen-bridged binuclear iron ions have been identified with various degrees of reliability. In contact with appropriate gases, $NO^+$ ions, mono- and dinitrosyl groups, nitro groups, nitrate ions and superoxide ions have been identified. Peroxide ions, though not detectable with the methods used here, were postulated by other authors on the basis of density functional calculations.

The binuclear iron oxo-ions are more abundant in the best catalysts with high Fe/Al ratio that were prepared by sublimation. They are the most probable sites for NO oxidation to $NO_2$ and its further conversion to adsorbed nitro groups and nitrate ions, steps that are crucial for $NO_x$ reduction. Superoxide and/or peroxide ions are likely involved in the NO oxidation to $NO_2$. This process is fast when Fe/MFI is exposed to a mixture of $NO + O_2$, but much slower if NO is chemisorbed first, before exposure to $O_2$. 

*Keywords:* SCR of $NO_x$; Fe/MFI catalysts; Binuclear iron oxo-ions; NO oxidation and adsorption; Superoxide/peroxide ions

## 1. Introduction

Zeolite MFI supported iron catalysts have recently attracted considerable attention. At low iron loading, Fe/MFI has been reported to be active for the partial oxidation of benzene to phenol and of methane to methanol with $N_2O$ as the oxidant [1]. With high iron loadings, certain "over-exchanged" Fe/MFI catalysts have demonstrated high activity and remarkable stability for the selective catalytic reduction (SCR) of $NO_x$ by hydrocarbons in the presence of a large excess of oxygen and water vapor [2,3].

As to the nature of the active sites, binuclear iron complexes have been proposed by several researchers. In Fe/MFI with low iron loading, Panov et al. [1,4], Sobolev et al. [5] and Ovanesyan et al. [6] found that a particular state of adsorbed oxygen, called α-oxygen, is important. They believe that this α-oxygen is associated with binuclear Fe complexes. For over-exchanged Fe/MFI, Feng and Hall [2] and Hall et al. [7] and our group [3,8] have suggested that

* Corresponding author. Tel.: +1-847-491-5263; fax: +1-847-467-1018.

*E-mail address:* wmhs@nwu.edu (W.M.H. Sachtler).

1381-1169/00/$ - see front matter 
PII: S1381-1169(00)00287-9

two iron ions are involved in a redox cycle during the SCR of $NO_x$. An oxygen-bridged binuclear iron complex $[HO–Fe–O–Fe–OH]^{2+}$ was proposed in our previous papers. This model permits a simple rationalization of the $H_2$-TPR and CO-TPR data and correctly describes the maximum metal loading with $Fe/Al = 1$. It also explains the thermal reduction behavior, as the bridging oxygen can be thought to be desorbed, thus reducing the two iron ions from $Fe^{3+}$ to $Fe^{2+}$. Desorption of oxygen from Fe/MFI prepared by hydrothermal synthesis was observed by Lázár et al. [9], who also proposed an Fe–O–Fe pair as the redox center.

Other models of the active sites in Fe/MFI catalysts for the SCR of $NO_x$ have also been proposed: Kucherov et al. [10], who quote ESR evidence, and Lee and Rhee [11], who considered isolated $Fe^{3+}$ ions as active sites. Joyner and Stockenhuber [12] did extended X-ray absorption fine structure (EXAFS) work on catalysts of low SCR activity and proposed $Fe_4O_4$ nano-clusters as active sites, while conceding, however, that the state of the iron will strongly depend on the preparation method.

Previously, we developed a sublimation method to prepare Fe/MFI with high iron loading ($Fe/Al \approx 1$) and high SCR activity. Immediately after sublimation, iron ions are found to be homogeneously distributed inside the zeolite cavities, compensating the negative charge of the zeolite framework. In following hydrolysis and calcination steps, the majority of iron ions remain at the exchange sites, though part of them aggregate forming microscopic "rafts" of iron oxide on the zeolite support [3]. Recently, we found that a treatment with an aqueous NaOH solution transforms iron ions in Fe/MFI to larger aggregates, which appear as iron oxide clusters after calcination. These clusters are still located inside zeolite channels, as follows from their re-dispersion back to the exchange sites when $Na^+$ ions are replaced by protons [13]. Catalytic tests show that iron oxide clusters have low activity for the SCR of $NO_x$, because they form little nitro and nitrate ($NO_y$, $y \geq 2$) chemisorption complexes at their surface. In contrast, formation of such $NO_y$ complexes is rather easy on Fe/MFI. This is of relevance because the $NO_y$ groups have been shown to be crucial for the SCR of $NO_x$ with hydrocarbons. Two issues requiring further clarification are (1) the precise nature of the sites and (2) the mechanism by which $NO_y$ complexes are formed.

In the present work, X-ray absorption spectroscopy (EXAFS and XANES) and ESR have been used to identify the iron sites over Fe/MFI. Since several different iron components will actually coexist in this catalyst, other samples used in our previous work have also been included for comparison. The adsorption of NO and $NO + O_2$ on these catalysts was followed by FTIR to identify the activity of each iron component. A relationship between the iron sites and their catalytic activities will be established.

## 2. Experimental

### *2.1. Catalysts preparation*

The zeolite MFI support used in this study was provided by UOP ($Si/Al = 14$, $Na/Al = 0.67$, lot # 13923-60). It was first converted into H/MFI by conventional ion exchange with a dilute $NH_4NO_3$ solution, followed by calcination up to 550°C. Fe/MFI was prepared by the sublimation technique describe previously [3,14]. In brief, $FeCl_3$ was sublimed into the cavities of H/MFI, where the chemical reaction $H^+ + FeCl_3 = [FeCl_2]^+ + HCl(gas)$ took place. After replacing all protons by $[FeCl_2]^+$, the sample was hydrolyzed and washed with DDI $H_2O$ to replace chlorine with hydroxyl groups. Finally, the Fe/MFI was dried and calcined in $O_2$ at 550°C for 4 h. A portion of the calcined Fe/MFI was suspended in an NaOH solution at $pH = 10.0$ and stirred overnight at room temperature. After filtration, the solid was thoroughly washed with DDI $H_2O$ and dried in air. After calcination in $O_2$ at 550°C for 4 h this sample, hereafter called Fe,Na/MFI, contains Fe in the form of ferric oxide nano-clusters. One portion of this Fe,Na/MFI was re-exchanged with a dilute $NH_4NO_3$ solution to displace the $Na^+$ ions by $NH_4^+$ ions. This procedure was repeated three times to ensure complete displacement. The sample was subsequently calcined in $O_2$ at 550°C for 4 h to convert $NH_4^+$ ions to protons; it will be called Fe,H/MFI. As a reference, an $Fe_2O_3$/HMFI was prepared by impregnating a certain amount of

$Fe(NO)_3$ onto H/MFI, which was followed by a calcination at 550°C for 4 h.

### 2.2. EXAFS and XANES

EXAFS and X-ray absorption near edge spectroscopy (XANES) at the K-edge of Fe were performed at DND CAT in Argonne National Laboratory (US). The Si(111) double crystal monochromator was detuned to 75% intensity to minimize the presence of higher harmonics. Data were collected at room temperature in the transmission mode using three optimized chambers as detectors and Fe metal foil as reference for energy correction.

The catalysts were pressed into self-supporting wafers, and the thickness of the wafers was adjusted to give an absorbency of 2.5. The wafers were dehydrated in an $O_2$ flow at 500°C for 4 h. After cooling in a glove bag filled with dry nitrogen, the pellets were transferred into sample holders sealed with kapton film windows. For Fe/MFI and Fe,Na/MFI samples, spectra were also recorded after the calcined wafers were contacted with liquid water.

The data were processed using a PC-based EXAFS analysis program from Tolmar Instruments (Ontario, Canada).

### 2.3. ESR

The ESR spectra were recorded on a Varian E-4 spectrometer at 9.3 GHZ (X band). The samples were dehydrated in $O_2$ at 500°C for 4 h. Measurements for each sample were carried out at room temperature and −196°C.

### 2.4. FTIR

Spectra were registered on a Nicolet 60 SX FTIR spectrometer using a liquid $N_2$-cooled MCT detector. The samples were pressed into self-supporting wafers of 8 mg/cm$^2$ and placed into a flow-through quartz cell sealed with NaCl windows. Typically, the sample was pretreated up to 500°C under flow of 5% $O_2$/He for 1 h, and cooled to room temperature in the same flow. For NO adsorption, the sample was purged with He for 0.5 h before 0.5% NO/He was introduced into the cell at a flow rate of 100 ml/min; For $NO + O_2$ adsorption, the sample was directly exposed to 0.5% $NO + 2\%$ $O_2 + He$ at the same flow rate. For Fe/MFI, such measurements were also done with the reduced sample. In such case, the Fe/MFI sample wafer was first reduced with 5% $H_2$/He (100 ml/min) at 400°C for 1 h and the flow gas was switched to He while the temperature was held at 400°C for an additional 0.5 h before cooling to room temperature. All spectra were recorded at room temperature as a function of exposure time. Fifty scans were accumulated with a spectral resolution of 1 cm$^{-1}$. A reference spectrum of the sample before exposure of NO or $NO + O_2$ was subtracted from each spectrum.

### 2.5. Oxidation of NO to $NO_2$

All samples were tested in a microflow reactor for the catalytic oxidation of NO to $NO_2$. The feed was provided from a set of mass flow controllers. The gas composition was 0.2% $NO + 3\%$ $O_2$ and the balance He. A sample of 0.10 g catalyst was used with a total flow rate of 140 cm$^3$/min, resulting in a GHSV = 42,000 h$^{-1}$. This condition was chosen to mimic that used in our previous work on the SCR of $NO_x$ with hydrocarbons [3]. The reaction temperature was increased stepwise from 200°C to 500°C. The products were flowed through an FTIR cell. The extinction coefficients of NO at 1900 cm$^{-1}$, and of $NO_2$ at 1630 cm$^{-1}$ were used to calculate the relative concentrations. A blank test with an empty reactor showed that the conversion of NO to $NO_2$ by homogeneous oxidation in the flow system and infrared cell was ∼2%. This background was subtracted from the conversion rates in the presence of a catalyst.

All the gases used in this study were UHP grade and further purified by passing the flow through a set of traps. A 2% NO in He was passed through two traps filled with glass beads at −80°C to remove $NO_2$ and $N_2O$ impurities.

## 3. Results

Table 1 gives the chemical composition of the four samples, with data from our previous papers

Table 1
Summary of catalyst characteristics

| Sample | Fe/Al[a] | Na/Al[a] | Brønsted acid sites (%)[b] | Desorbed $O_2$ (O/Fe)[c] |
|---|---|---|---|---|
| Fe/MFI | 1.00 | – | 25 | 0.108 |
| Fe,Na/MFI | 0.92 | 0.45 | – | 0.026 |
| Fe,H/MFI | 0.91 | – | 40 | |
| $Fe_2O_3$/HMFI | 1.00 | – | 90 | 0.020 |

[a] Mole ratio determined by ICP analysis.
[b] Relative intensity of Brønsted acid sites measured by IR band at 3610 $cm^{-1}$. The intensity of the Brønsted acid sites in parent H/MFI was counted as 1 (see Ref. [13]).
[c] The amount of $O_2$ desorbed in a thermal reduction (see Ref. [8]).

also included. The intensity of Brønsted acid sites was determined by the IR band at 3610 $cm^{-1}$ [13]; the amount of desorbed $O_2$ was measured by thermal reduction [8]. Though the Fe/Al ratio in Fe/MFI is unity, the sample still contains 25% protons. This indicates that not all of the iron ions are located at the exchange sites: Some aggregation has taken place. This is confirmed by TEM results reported in our previous work [3]. When the sample was treated with NaOH, the $Na^+$ ions displaced not only the protons, but also some iron ions from exchange sites. However, the total iron content of the sample did not decrease significantly. This strongly indicates aggregation of iron ions. In a following re-exchange step, the $Na^+$ ions could be completely exchanged against $NH_4^+$, again without losing significant amounts of Fe. Upon calcination, ammonium ions were converted to protons, but their number is lower (40%) than that of the displaced $Na^+$ ions (45%). It follows that some protons have reacted with the iron oxide so that iron ions returned to the exchange sites. It follows that the previous agglomeration process caused by NaOH has, in part, been reversed. Such "protonolysis" was also found to take place during calcination of $Fe_2O_3$/HMFI [15].

### 3.1. EXAFS and XANES

Fourier transforms of the calcined samples and of bulk $Fe_2O_3$ are shown in Fig. 1. It is obvious that the features of $Fe_2O_3$/HMFI closely resemble that of bulk $Fe_2O_3$, indicating that in $Fe_2O_3$/HMFI the majority of iron is present as small $Fe_2O_3$ particles that will be located at the external surface of the zeolite. The features of the other three samples, however, are significantly different: the first coordination shell is narrow, while the second one is much weaker, indicating that the majority of iron in these three samples is highly dispersed. A quantitative EXAFS data analysis was not done, because different coordination states of iron co-exist in a priori unknown concentrations in each of these samples; for some components the coordination environment

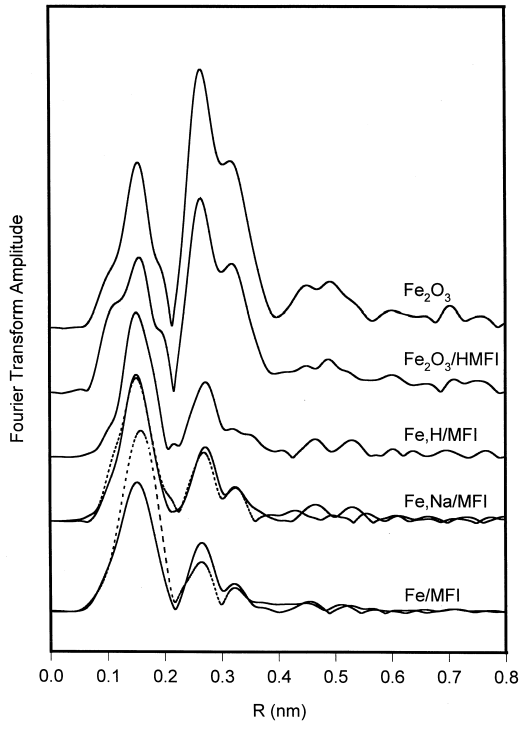


Fig. 1. Fourier transformed Fe K-edge $\chi(k) * k^2$ EXAFS spectra of calcined samples (solid line); and re-hydrated samples (dashed line).

will be highly disordered. In this situation, a quantitative EXAFS analysis, providing only average coordination numbers and distances, would have little physical meaning. This is underscored by the fact that two catalysts with profoundly different catalytic activities, Fe/MFI and Fe,Na/MFI, [13,14], display very similar EXAFS spectra (Fig. 1). We have, therefore, refrained from fitting the spectra to simulated model curves.

Although the radial distribution function of dehydrated Fe/MFI is very similar to that of calcined Fe,Na/MFI (see Fig. 1), different features were observed upon completely re-hydrating the samples. The spectrum of Fe,Na/MFI showed almost no change after hydration, but large changes were found when a dehydrated pellet of Fe/MFI was contacted with liquid water. This not only increases the first coordination shell of the iron centers, but also decreases the second shell.

As XANES spectroscopy can provide important information about the local atomic coordination state and its changes upon interaction with adsorbates, it was included in this study. The spectra are shown in Fig. 2. The small pre-edge peak is assigned to 1s → 3d transitions [16,17]. Systems with octahedral symmetry do not show such peaks, while systems with tetrahedral symmetry give a rather intensive one. Similar to the EXAFS results shown in Fig. 1, the XANES spectra in Fig. 2 show nearly identical features for $Fe_2O_3$/HMFI and bulk $Fe_2O_3$. For the other three dehydrated samples, the spectra resemble each other, but they are somewhat different from that of $Fe_2O_3$. The spectra of all these samples are different from that of $Fe_3O_4$, suggesting that Fe is in the oxidation state of $Fe^{3+}$. The rather intensive pre-edge peak observed over Fe/MFI, Fe,Na/MFI, and Fe,H/MFI indicates a high percentage of non-octahedral (presumably tetrahedral) coordinated iron in these samples. Upon adding water, the pre-edge peak of Fe/MFI decreased by ~25%, but only a marginal change was observed with Fe,Na/MFI. Both XAFS techniques, EXAFS and XANES, suggest that the iron ions in Fe,Na/MFI, though coordinately unsaturated, are rather "inert" toward ligation. This distinguishes them from the iron ions in Fe/MFI, which eagerly form bonds with guest ligands, resulting in de-anchoring of the iron ions.

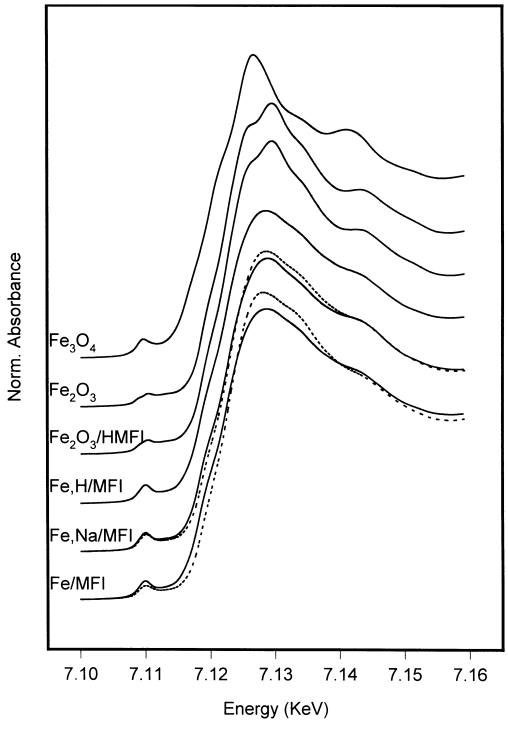


Fig. 2. XANES of calcined samples (solid line); and re-hydrated samples (dashed line).

### 3.2. ESR

ESR spectra of the samples were recorded at room temperature and at −196°C. As can be seen from Fig. 3, Fe/MFI shows five signals at $g = 6.3$, 5.6, 4.3, 2.3 and 2.03 at room temperature. Upon cooling to −196°C, the signals at $g > 3$ remains, but those at $g < 3$ are no longer visible. Instead, a very sharp line at $g = 2.0$ appears. Signals in the low field region ($g > 3$) are usually attributed to isolated $Fe^{3+}$ ions in different coordination environments. The $g = 4.3$ signal is due to $Fe^{3+}$ ions in a strong rhombic distortion of the tetrahedral site, while the $g = 5.6$ and 6.3 signals are attributed to $Fe^{3+}$ ions in a less distorted tetrahedron that maintains a $C_{3v}$ axial symmetry [10,11,16,18]. The line at $g = 2.3$ is very broad, and a similar line was observed over $Fe_2O_3$/HMFI, which can be attributed to iron in small $Fe_2O_3$ particles. The signals at $g = 2.03$ and $g = 2.3$ disappear at −196°C, and do not follow

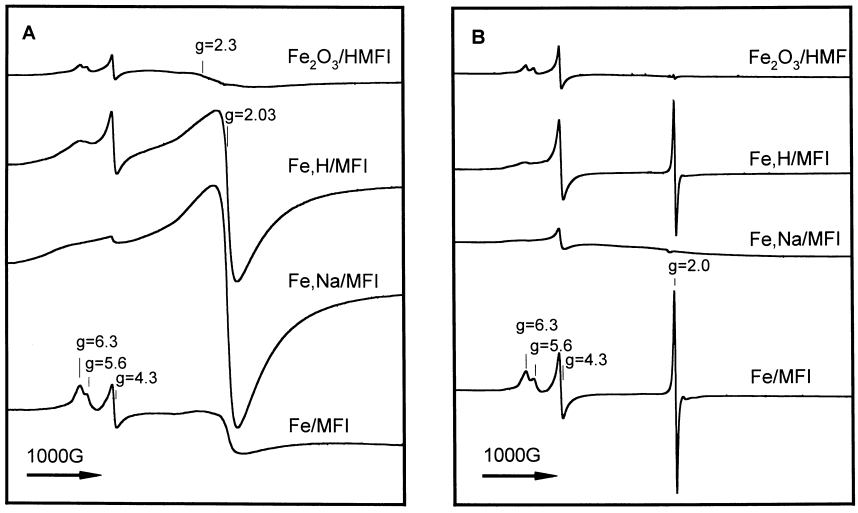


Fig. 3. ESR spectra of calcined samples recorded at room temperature (A); and −196°C (B).

Curie's law, indicating that the corresponding $Fe^{3+}$ ions are in mutual magnetic interaction. The signal at $g = 2.03$ can be attributed to a separate antiferromagnetic Fe–O–Fe phase [19–21]. This could consist of ferric oxide nano-clusters inside the zeolite channels; these clusters could exhibit superparamagnetic or even ferromagnetic behavior [16]. Another possibility is binuclear iron ions $[HO–Fe–O–Fe–OH]^{2+}$ at the exchange sites [18]. The sharp line at $g = 2.0$, observed only at −196°C, is very sensitive to ligands and disappears upon adsorption of $H_2O$ or $NH_3$. We attribute it to superoxide ions $(O_2^-)$, which are associated with iron ions. A similar line was observed over V-ZSM-22, and was assigned to $O_2^-$ [22].

The ESR spectrum of Fe,Na/MFI at room temperature is dominated by an intensive signal at $g = 2.03$. Those lines attributed to isolated $Fe^{3+}$ ions are hardly visible; the $g = 2.3$ signal is masked by the intensive $g = 2.03$ line. Both of them disappear at −196°C. As discussed above, they can be attributed to small $Fe_2O_3$ particles on the external surface of zeolite and ferric oxide nano-clusters inside the zeolite channels, respectively.

Replacing $Na^+$ ions by $NH_4^+$, followed by calcination, re-disperses part of the iron ions, as evidenced by the ESR spectra of Fe,H/MFI presented in Fig. 3. The signal at $g > 3$, which is due to $Fe^{3+}$ ions in isolated states reappears. Also, at −196°C, the sharp line at $g = 2.0$ that is assigned to superoxide ions $(O_2^-)$ reappears.

The ESR spectra of $Fe_2O_3$/MFI show not only the $g = 2.3$ signal that is attributed to small $Fe_2O_3$ particles, but also signals at $g > 3$. This confirms that solid state ion exchange had occurred. Protons in the zeolite support dissolve part of $Fe_2O_3$ [15].

### 3.3. FTIR

In this study, NO is used as a probe molecule to identify the active sites over the iron catalysts. This technique has been widely used in literature [23–31]. Since NO is found to be adsorbed more strongly over $Fe^{2+}$ sites than $Fe^{3+}$ sites, a reduced Fe/MFI sample was also included.

#### 3.3.1. Exposure to NO

IR spectra of NO adsorbed on reduced Fe/MFI are shown in Fig. 4. These spectra are similar to the results reported in the literature [23–31]. In the presence of NO, three major bands are observed at 2133, 1882, and 1809 $cm^{-1}$ with three shoulders at 1918, 1858, and 1770 $cm^{-1}$. The bands at 1882 and 1858 $cm^{-1}$ are assigned to mononitrosyl complexes $[Fe^{2+}(NO)]$ with $Fe^{2+}$ ions located at different exchange sites. The bands at 1918 and 1809 $cm^{-1}$ are assigned to $Fe^{2+}$ dinitrosyl complexes, $[Fe^{2+}(NO)_2]$, with $Fe^{2+}$ ions in well-accessible positions. The

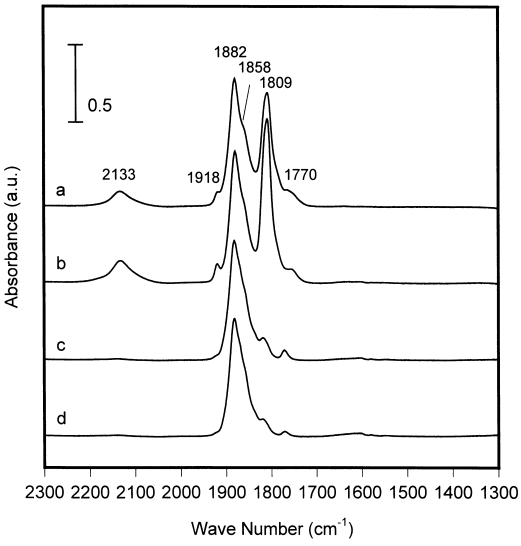


Fig. 4. IR spectra upon exposing reduced Fe/MFI to 0.5% NO + He for 2 min (a); 30 min (b); followed by He purge for 30 min (c); and subsequent $O_2$ purge for 30 min (d).

corresponding iron mononitrosyl complex formed at the same iron sites gives rise to the 1770 $cm^{-1}$ band. The band at 2133 $cm^{-1}$ is assigned to $NO^+$ ions at cation exchange sites of MFI [31]. The bands at 1882 and 1858 $cm^{-1}$ are formed quickly upon exposure to NO and their intensity hardly changes thereafter even upon purging with He. Remarkably, they do not change even in the following purging with $O_2$. The bands of dinitrosyl also form rather quickly and their intensity continues to increase slowly with exposure time. However, upon purging with He, it decreases to a rather low value. The intensity of the 1770 $cm^{-1}$ band is rather low and difficult to determine. No large change was observed during NO adsorption and He purge, but upon purging with $O_2$ it decreased. The change of the intensity of the 2133 $cm^{-1}$ band, which disappears in He flow, will be discussed in Section 3.3.2.

Fig. 5 shows the spectra of NO adsorbed on oxidized Fe/MFI. Interestingly, all the bands appearing on the reduced sample (Fig. 4) are also observed with this oxidized sample at the same positions, but with different intensity. Comparison of Fig. 5a with Fig. 4a shows that in the oxidized sample the band at 1882 $cm^{-1}$ is 25% less intense. The intensity does not change with exposure time, but decreases slightly in flowing He. Since the position of this band is the same as that in the reduced sample, some authors attribute it to $Fe^{2+}(NO)$ [28–31]. However, Segawa et al. [25] found that the position of this band is rather insensitive to the valence state of iron; rather, it depends on the *location* of the Fe ions. As the intensity of this band is comparable in Figs. 4 and 5, we tend to agree with these authors and assign this band to an iron-nitrosyl: In the case of the oxidized sample in Fig. 5, this will be $Fe^{3+}(NO)$. The 1858 $cm^{-1}$ band is rather weak in Fig. 5. The dinitrosyl groups (1918 and 1809 $cm^{-1}$), usually formed on $Fe^{2+}$ sites, are also observed in Fig. 5, although with a much lower intensity compared with Fig. 4. $NO^+$ at the exchange sites (2133 $cm^{-1}$) appears quickly. After 30 min NO exposure, weak bands in 1650–1550 $cm^{-1}$ region emerge. Interestingly, these bands, especially the 1620 $cm^{-1}$ band that is assigned to $Fe^{n+}NO_2$ (see below), become more intensive after purging with He, but no further increase is observed when $O_2$ is admitted.

Upon exposing Fe,Na/MFI to NO, only weak bands are observed (Fig. 6). The band at 1878 $cm^{-1}$ increases slowly with exposure time, and shifts to

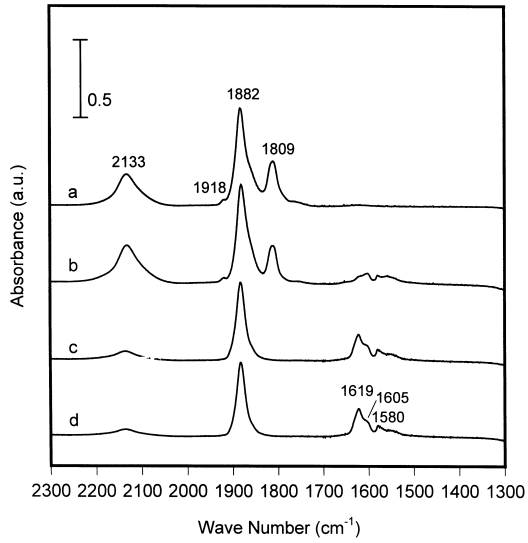


Fig. 5. IR spectra upon exposing oxidized Fe/MFI to 0.5% NO + He for 2 min (a); 30 min (b); followed by He purge for 30 min (c); and subsequent $O_2$ purge for 30 min (d).

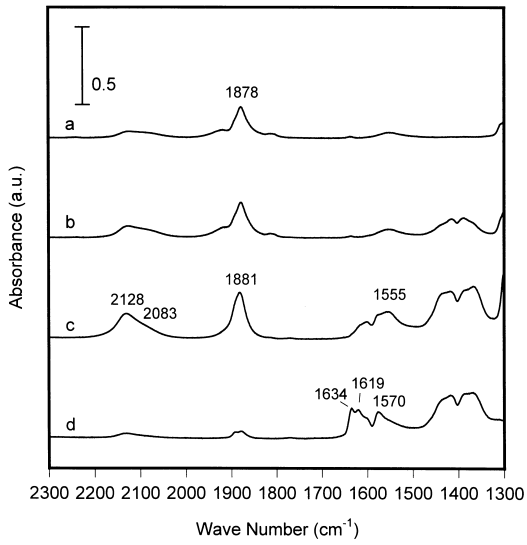


Fig. 6. IR spectra upon exposing Fe,Na/MFI to 0.5% NO + He for 2 min (a); 5 min (b); 30 min (c); and followed by He purge for 30 min (d).

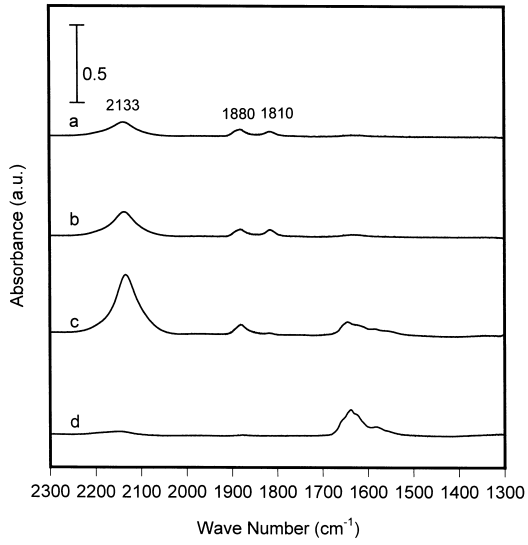


Fig. 7. IR spectra upon exposing $Fe_2O_3$/HMFI to 0.5% NO + He for 2 min (a); 5 min (b); 30 min (c); and followed by He purge for 30 min (d).

1881 $cm^{-1}$ after 30 min. The low intensity of this band is in agreement with the results reported in literature, i.e., NO can hardly be adsorbed on $Fe_2O_3$ either in the form of bulk oxide, or when it is highly dispersed [23–31]. Also, this band may contain contribution from adsorbed $N_2O_3$ [32]. Indeed, another band from $N_2O_3$ can be found at around 1555 $cm^{-1}$. In He flow, both the 1881 and 1555 $cm^{-1}$ bands decreases. The bands at 2128 $cm^{-1}$ with shoulder at 2083 $cm^{-1}$ increase with exposure time, but disappear upon purging. In the low frequency region, weak bands attributed to nitro/nitrate groups on either iron sites or $Na^+$ sites emerge. Interestingly, bands at 1634 and 1619 $cm^{-1}$ also increase upon purging.

When feeding NO to $Fe_2O_3$/HMFI, the main feature in the IR spectra is the band at 2133 $cm^{-1}$, which grows with exposure time (Fig. 7). The bands at 1880 and 1810 $cm^{-1}$ are very weak, and vanish in flowing He. Weak bands in the 1650–1550 $cm^{-1}$ region grow slowly with time, even during He purge.

The IR spectra measured upon exposing Fe,H/ZSM-5 to NO (or to NO + $O_2$, see Section 3.3.2) are quite similar to those recorded over Fe/MFI, except for slight changes of the relative intensities. Therefore, these spectra are not shown here.

### *3.3.2. Exposure to NO + $O_2$*

Exposure to a mixture of $O_2$ and NO at room temperature leads to remarkably different IR spectra than exposure to NO, followed by purging with $O_2$. Fig. 8 shows the spectra with Fe/MFI, and the

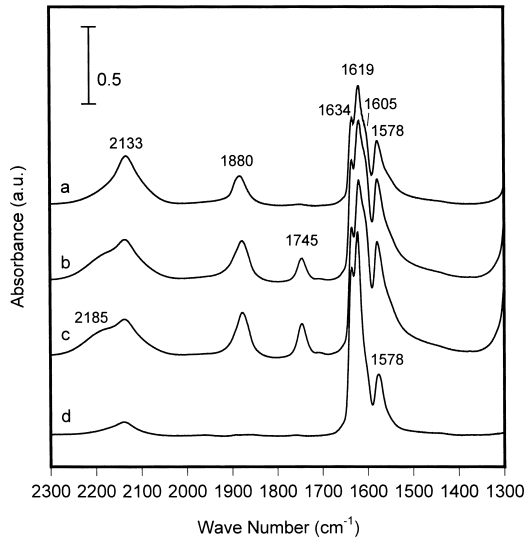


Fig. 8. IR spectra upon exposing Fe/MFI to 0.5% NO + 3% $O_2$ + He for 2 min (a); 5 min (b); 30 min (c); and followed by 3% $O_2$ + He purge for 30 min (d).

difference with Fig. 5 is striking. The band ascribed to $NO^+$ at 2133 $cm^{-1}$ reaches its maximum at 2 min. Although a band at 1880 $cm^{-1}$ is also observed, it seems better to assign it not to a mononitrosyl group but instead, to adsorbed $N_2O_3$, because the other band of this molecule, near 1578 $cm^{-1}$, is also rather intensive. The latter band actually overlaps with a band from a nitrate species at the same wave number (see below). The band at 1745 $cm^{-1}$ is from $N_2O_4$ [32], and grows with exposure time. Adsorbed $N_2O_4$ also shows another band at 2185 $cm^{-1}$, and Hadjiivanov et al. [30] assigned it to an $[NO^+][N_2O_4]$ adduct. Bands in the 1650–1550 $cm^{-1}$ region have been assigned to nitro and nitrate groups over iron sites in our previous work [33]. In that work, spectra were recorded at 200°C, and two bands at 1625 and 1570 $cm^{-1}$ were observed, which are attributed to nitro and nitrate groups, respectively. In Fig. 8, both bands appear at 1619 and 1578 $cm^{-1}$. The latter band overlaps with a band from $N_2O_3$. In addition, two shoulders appear at 1634 and 1605 $cm^{-1}$. The 1634 $cm^{-1}$ band might also be due to a nitro group bonded to an iron ion at a different location, while the 1605 $cm^{-1}$ band might be assigned to $NO_2$ weakly adsorbed on the ferric oxide nano-clusters (see below). Upon purging with $O_2$,

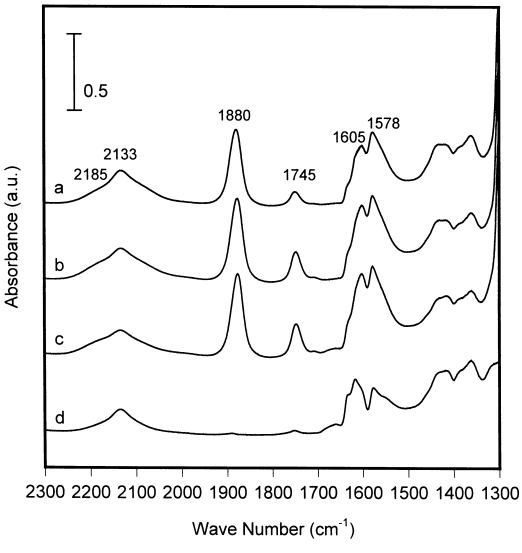


Fig. 9. IR spectra upon exposing Fe,Na/MFI to 0.5% NO + 3% $O_2$ + He for 2 min (a); 5 min (b); 30 min (c); and followed by 3% $O_2$ + He purge for 30 min (d).

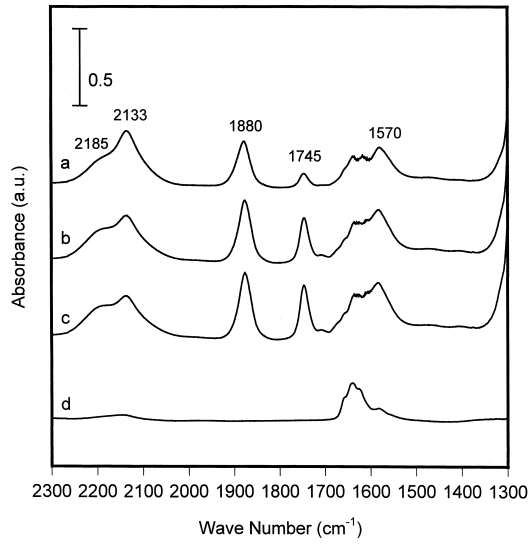


Fig. 10. IR spectra upon exposing $Fe_2O_3$/MFI to 0.5% NO + 3% $O_2$ + He for 2 min (a); 5 min (b); 30 min (c); and followed by 3% $O_2$ + He purge for 30 min (d).

$N_2O_3$ and $N_2O_4$ are desorbed, so the band observed at 1578 $cm^{-1}$ in Fig. 8d is the real band of a nitrate group. The response of those nitro groups toward purging is different: the band at 1605 $cm^{-1}$ decays, whereas the bands at 1634 and 1619 $cm^{-1}$ increase. This result together with the decrease of the $N_2O_3$ and $N_2O_4$ bands further support the assignment of the latter two bands to nitro groups. Our previous work [33], and also recent results of Lobree et al. [29] show that the nitro group at 1634 $cm^{-1}$ is less stable than the one at 1620 $cm^{-1}$: The 1634 $cm^{-1}$ band disappears at 200°C.

Exposing the reduced Fe/MFI to NO + $O_2$ yields an IR spectrum identical to that observed after exposure of the oxidized Fe/MFI. Apparently, the reduced and the oxidized Fe/MFI quickly reach the same state.

The IR spectra of Fe,Na/MFI in flowing NO + $O_2$ are shown in Fig. 9. Bands at 2133 $cm^{-1}$ ($NO^+$), 1880 and 1578 $cm^{-1}$ (adsorbed $N_2O_3$), and 2185 and 1745 $cm^{-1}$ (adsorbed $N_2O_4$) quickly appear. Actually, the bands assigned to adsorbed $N_2O_4$ appear even faster on Fe,Na/MFI than on Fe/MFI. However, the bands assigned to nitro groups on iron sites are rather weak and masked by the band at

1605 $cm^{-1}$. The latter band disappears when the NO flow is shut down. Since the majority of iron ions in this sample are ferric oxide nano-clusters, we tentatively assign this band to a nitro group that is weakly adsorbed on such clusters.

Fig. 10 shows the IR spectra measured over $Fe_2O_3$/HMFI exposed to NO + $O_2$. As with Fe,Na/MFI, bands of $NO^+$(2133 $cm^{-1}$), adsorbed $N_2O_3$ (1880, 1570 $cm^{-1}$), and adsorbed $N_2O_4$ (2185, 1745 $cm^{-1}$) appear rapidly. The bands assigned to nitro/nitrate groups on iron sites are even weaker than with Fe,Na/MFI. Actually, the IR spectrum d in Fig. 10 is almost identical to that observed over the parent H/MFI in the same atmosphere.

### 3.4. Oxidation of NO to $NO_2$

Oxidation of NO over the four catalysts was measured. The reaction conditions used here are almost the same as used previously for the SCR of NO with *iso*-$C_4H_{10}$. The only difference is that *iso*-$C_4H_{10}$ is replaced by an equal amount of helium. The $NO_2/(NO + NO_2)$ ratio is shown in Fig. 11 as a function of reaction temperature. In the same figure, the thermodynamic equilibrium value from Ref. [34] is shown as a dashed curve. It is very clear that

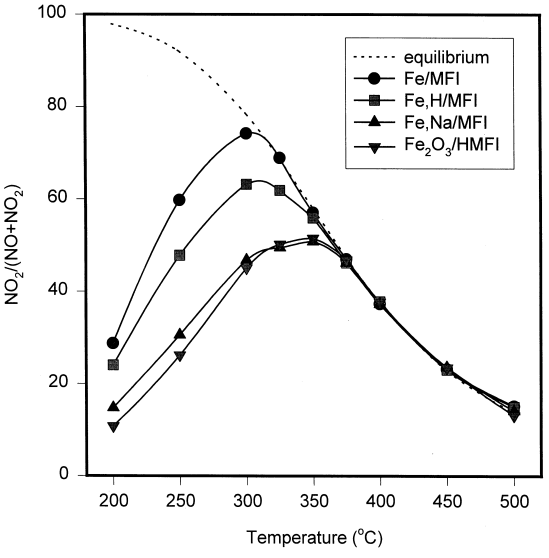


Fig. 11. Oxidation of NO to $NO_2$ as a function of reaction temperature over different catalysts feed: 0.2% NO + 3% $O_2$ + He; flow rate: 140 ml/min; catalyst: 0.1 g; GHSV = 42,000 $h^{-1}$.

Fe/MFI is the most active catalyst, followed by Fe,H/MFI. The activities of Fe,Na/MFI and $Fe_2O_3$/HMFI are similar to that of Fe,Na/MFI, but much poorer than that of Fe/MFI.

## 4. Discussion

The ESR results in Fig. 3 clearly show that different iron components coexist in each catalyst. Their relative concentrations strongly depend on the preparation conditions, but it is not easy to obtain reliable quantitative values. As mentioned, we are therefore refraining from quantitative spectral fitting of the EXAFS results shown in Fig. 1. However, a qualitative analysis of the EXAFS data is quite instructive about the nature of the iron sites in each of the catalysts.

For a quantitative EXAFS study on Fe/MFI catalysts, the reader is referred to recent papers by Joyner and Stockenhuber [12], and Marturano et al. [35]. The former group used EXAFS to examine Fe/MFI catalysts prepared by various ion exchange methods. Like us, they found that isolated iron ions, iron oxo-nanoclusters, and microscopic iron oxide particles coexist in their samples. They believe, however, that their EXAFS quantitative analysis is consistent with iron oxo nanoclusters of an average composition of $Fe_4O_4$. These clusters have rather short Fe–Fe distances; they were proposed to be the active sites for the SCR of $NO_x$. Unfortunately, these samples had a much lower Fe loading than those of the present study and they displayed a lower SCR activity than is typical for over-exchanged metal/zeolite catalysts. Recently, Marturano et al. used EXAFS to examine Fe/MFI samples prepared by the sublimation method. They measured EXAFS at −196°C to minimize effects caused by thermal disorder and found that the state of iron depends on the zeolite batch used. For a sample with highly dispersed iron, best fit with the measured spectrum is obtained with the model of the binuclear Fe–O–Fe complex [35].

### 4.1. Iron components in different catalysts

$Fe_2O_3$/HMFI prepared by impregnation shows EXAFS and XANES spectra similar to those of bulk

$Fe_2O_3$. This illustrates that small $Fe_2O_3$ particles on the external surface of the zeolite support are predominant in this sample. Although solid state exchange does also occur, which introduces some iron ions into the zeolite exchange sites (see ESR spectra in Fig. 3), this exchange remains below 10%, as follows from the intensity of the IR bands of the Brønsted acid sites listed in Table 1.

The EXAFS spectra of Fe,Na/MFI indicate that iron is highly dispersed, as follows also from the ESR signal at $g = 2.03$, which does not follow Curie's law. This behavior is typical for superparamagnetic or ferromagnetic ferric oxide nano-clusters. The ESR spectra indicate negligible concentration of isolated iron ions in this sample. They do not exclude the presence of a few small $Fe_2O_3$ particles, because the signal at $g = 2.3$ is masked by the intensive signal at $g = 2.03$. In this sample, no Brønsted acid sites have been detected by IR although the amount of sodium ions can only compensate the charge of 45% of the Al-centered tetrahedra. Therefore, these ferric oxide nano-clusters are still inside the zeolite channels and carry a positive charge compensating the other 55% of the negative charge of the zeolite framework. Upon assuming that each sodium ion occupies one exchange site, it follows that two iron ions should balance the charge of one Al-centered tetrahedron. The rather intensive pre-edge peak in its XANES spectrum points to such clusters with low coordination symmetry. Interestingly, they hardly change upon adding $H_2O$ ligands, as demonstrated by the EXAFS results in Fig. 1 and the XANES spectrum in Fig. 2. One possibility might be that these iron ions form a kind of network inside zeolite channels. Such a structure might hold them together in the presence of guest ligands.

Upon displacing $Na^+$ by $NH_4^+$, followed by calcination, protons of high acidity are generated, which etch part of these ferric oxide nano-clusters. The resulting iron ions will re-disperse in the zeolite, and isolated iron ions in exchange positions are formed as shown in Fig. 3.

Fe/MFI prepared by sublimation also contains some isolated iron ions, ferric oxide nano-clusters and small $Fe_2O_3$ particles, as shown in Fig. 3. A unique feature of this catalyst is that upon adding $H_2O$ ligands, the coordination symmetry of the iron ions changes from tetrahedral to octahedral (Fig. 2) and the coordination number of the iron with ligands in the first shell increases markedly (Fig. 1). For isolated iron ions, this would be trivial, but the simultaneous decrease of the second coordination shell requires a different explanation. In our previous work, we had proposed an oxygen-bridged binuclear iron complex $[HO–Fe–O–Fe–OH]^{2+}$ as the active site in Fe/MFI [3]. It appears that the present EXAFS data can be rationalized in terms of this model. The iron ions in such a complex will be coordinatively unsaturated; addition of water will presumably replace the bridging oxygen by two hydroxyl groups and thus increase the coordination number. As a result, the two iron ions lose their mutual contact, and coordination in the second shell will decrease, while the first shell coordination increases, in agreement with the EXAFS and XANES data.

Binuclear iron complexes have been claimed to be the active centers in the enzyme methane monooxygenase [36,37]. This enzyme can activate $O_2$ at ambient temperature. A similar structure has been proposed by Panov et al. [1] for the active sites in an Fe/MFI catalyst that catalyzes the oxidation of methane and benzene with $N_2O$. They suggest that the iron pairs are ESR-silent [5]. This indicates analogy with the binuclear $[Cu–O–Cu]^{2+}$ ion in Cu/MFI for which Lei et al. [38] found that it is ESR silent. Recently, El-Malki et al. [18] stated that binuclear iron complexes $[HO–Fe–O–Fe–OH]^{2+}$ in exchange sites cause an ESR signal at $g = 2.03$ at room temperature, which disappears at $-196$°C. This is in line with the present ESR results in Fig. 3.

It is remarkable that the ESR spectra of Fe/MFI and Fe,H/MFI show a sharp line at $g = 2.0$ at $-196$°C, which is assigned to superoxide ions ($O_2^-$) associated with iron ions. This line is not found over the other two samples. It follows that in the former samples the Fe ions are accessible to $O_2$ and able to form charge transfer complexes with it. Our previous work shows that Fe/MFI can release part of its oxygen by simply heating in a flow of He [8]. The amount of $O_2$ released from these materials is much larger than that desorbed from Fe,Na/MFI and $Fe_2O_3$/HMFI (see Table 1). It is therefore plausible that the same iron center is responsible for the formation of superoxide ions and the release of $O_2$ upon heating. These results can be rationalized in terms of the binuclear model. Since the bridging

oxygen is rather labile, it can be thermally desorbed as discussed previously [8]. In the presence of $O_2$, the following reaction might be possible:

$$[HO–Fe^{2+}–\square–Fe^{2+}–OH]^{2+} + O_2 = [HO–Fe^{2+} \cdots O^{2-}–Fe^{3+}–OH]^{2+}. \quad (1)$$

The vacancy in the binuclear site will be regenerated when $O_2$ is released. Interaction with $H_2O$ would release $H_2O_2$, while regenerating $[HO–Fe^{3+}–O–Fe^{3+}–OH]^{2+}$.

On Fe/MFI, the $O_2^-$ radical is sufficiently stable to be observed by ESR at $-196$°C. At higher temperature, it might still be present as a reactive, though short-lived reaction intermediate. On Cu/MFI, the IR evidence for the formation of superoxide ions was obtained by Sárkány and Sachtler [39] and Sárkány [40] at room temperature. They attribute an IR band at 2294 $cm^{-1}$ to $[Cu^{2+}–O_2^- \cdots Cu^+]^{2+}$, another binuclear center in zeolite MFI.

### 4.2. Relationship between iron sites and $NO_x$ adsorption

IR spectra in Figs. 7 and 10 show that $Fe_2O_3$/HMFI does not adsorb appreciable amounts of nitrosyl, nitro, and nitrate groups. As this material contains mainly small $Fe_2O_3$ particles, one can reasonably conclude that such $Fe_2O_3$ particles do not chemisorb significant amounts of NO or $NO_2$. This is in agreement with results reported by other authors [24,41]. Accordingly, only very weak IR bands of adsorbed $NO_x$ are observed on Fe,Na/MFI (Figs. 6 and 9). As this material mainly contains ferric oxide nano-clusters, these can also be disregarded as active sites. It is more difficult to eliminate isolated iron ions as potential catalytic sites for SCR of $NO_x$. There is, however, a consensus that Fe/MFI catalysts with low Fe loading, as prepared by wet ion exchange, are very poor SCR catalysts, and metal loading in over-exchanged samples is essential. In the present work, the absence of characteristic IR bands on $Fe_2O_3$/HMFI, a material which undoubtedly contains isolated iron ions, indicates that isolated Fe ions are unlikely to be able to strongly chemisorb NO or $NO_2$. This follows from a comparison of Figs. 5 and 8, where strong $NO_x$ adsorption on Fe/MFI is evident.

Four kinds of iron sites appear to coexist in Fe/MFI: small $Fe_2O_3$ oxide crystals, ferric oxide nano-clusters, isolated iron ions, and oxygen-bridged binuclear iron ions. After elimination of the former three as centers for strong chemisorption of NO and $NO_2$, it is concluded that the binuclear ions $[HO–Fe–O–Fe–OH]^{2+}$ are the most active sites for $NO_x$ adsorption.

### 4.3. Catalysis on $[HO–Fe–O–Fe–OH]^{2+}$ model

It is interesting that the band at 2133 $cm^{-1}$ appears in all NO adsorption experiments. This band has been assigned to $NO^+$ at cation exchange positions of the MFI zeolite. It is not clear which electron acceptors convert NO to $NO^+$. $Fe^{3+}$ ions are obvious candidates; indeed the band is stronger on the calcined than on the reduced catalyst. Although oxygen traps were used in the present work, it cannot be excluded that traces of oxygen are able to pass through the traps. As all data were collected under flow conditions, a very low partial pressure of $O_2$ could suffice to oxidize some $Fe^{2+}$ to $Fe^{3+}$ and NO to $NO_2$. Hadjiivanov et al. [31] showed that $NO^+$ is formed by the following reaction:

$$NO + NO_2 + 2H^+ = 2NO^+ + H_2O. \quad (2)$$

In runs where only NO is admitted, the $NO_2$ required for reaction (2) would be formed by catalytic oxidation of NO with trace oxygen. There is indeed ample evidence that this oxidation is effectively catalyzed over sites such as

$$[HO–Fe^{3+}–O–Fe^{3+}–OH]^{2+}:$$

$$[HO–Fe^{3+}–O–Fe^{3+}–OH]^{2+} + NO = [HO–Fe^{2+}–\square–Fe^{2+}–OH]^{2+} + NO_2. \quad (3)$$

In Fig. 12, the normalized intensities of the 2133 $cm^{-1}$ band are plotted versus time. The graph shows that the rate of $NO^+$ formation is indeed highest over the catalysts with highest activity for the oxidation of NO to $NO_2$.

A second interesting feature of Fe/MFI is the appearance of dinitrosyl groups (1918, 1809 $cm^{-1}$). As these groups are believed to be formed on $Fe^{2+}$, part of the iron is reduced from $Fe^{3+}$ to $Fe^{2+}$ during NO adsorption in accordance with Eq. (3). The most

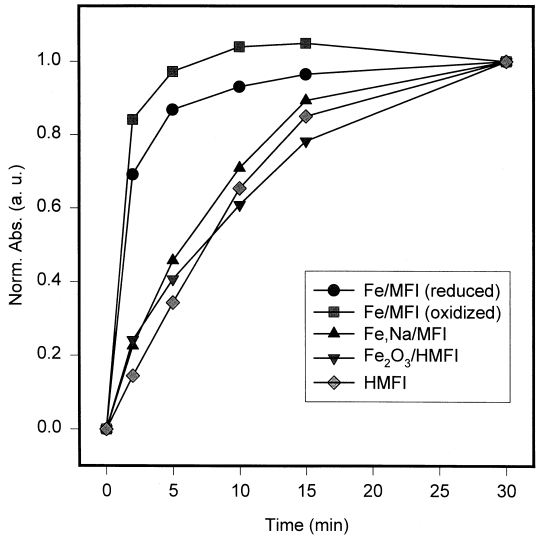


Fig. 12. The normalized intensity of the 2133 $cm^{-1}$ IR band as a function of exposure time over different catalysts.

favorable position for a binuclear iron complex in zeolite MFI is in the zeolite channels, or so-called γ sites [42]. Reaction (3) creates two $Fe^{2+}$ ions on highly accessible positions, which is ideal for the formation of dinitrosyl groups.

Oxidation with $O_2$ is not the only way to oxidize $Fe^{2+}$ to $Fe^{3+}$. Fu et al. [43] showed that NO acts as an oxidant in FeY where a binuclear iron complex has also been proposed. A reaction where two NO molecules are transformed to one $N_2O$ molecule and an adsorbed oxide ion was demonstrated by Lei et al. [38] over Cu/MFI containing $[Cu–O–Cu]^{2+}$ ions.

The third interesting result in Fig. 5 is that the nitro and nitrate groups (1650–1550 $cm^{-1}$) form slowly in the presence of NO. However, the corresponding band intensities increase upon purging with He, especially that of the 1619 $cm^{-1}$ band of a nitro group on an iron site. At the same time, the bands of the dinitrosyl groups disappear. These results suggest that the nitro/nitrate groups and the dinitrosyl groups are ligated to the same iron sites.

An important finding of significance for the mechanism is illustrated in Fig. 5. Once NO is adsorbed at the other iron sites, which show IR bands at 1882 and 1858 $cm^{-1}$, it will not be oxidized by $O_2$ to nitro or nitrate groups. However, when NO and $O_2$ are *both* present in the gas phase, such adsorption complexes are immediately formed on Fe/MFI, regardless of the initial iron valence state of the iron. The same result was recently reported by Lobree et al. [29]. These authors speculate that a superoxide ion ($O_2^-$) is involved in the formation of such nitro and nitrate groups. The ESR results in the present work support such a reaction mechanism:

$$\left[HO–Fe^{2+} \cdots O_2^- –Fe^{3+}–OH\right]^{2+} + NO = \left[HO–Fe^{2+}\right]^{+} + \left[NO_3^- –Fe^{3+}–OH\right]^{+} \quad (4)$$

$$\left[HO–Fe^{2+}\right]^{+} + NO_2 = \left[HO–Fe–NO_2\right]^{+}. \quad (5)$$

The superoxide ion in reaction (4) can be formed according to reaction (1).

Superoxide ions are not stable; on FeMFI they have only been observed by ESR at low temperature. However, the time between adsorption of an $O_2$ molecule and subsequent impact of an NO molecule onto the same site will be shorter than a microsecond. It is therefore conceivable that a fraction of the impinging NO molecules will hit $O_2^-$ ions.

On Ba/MgO catalyst, Mestl et al. also found that the presence of $O_2$ enhances the activation of NO to form the active Ba-nitro intermediate. By using in situ Raman spectroscopy, they found that surface peroxide ions on defect-rich BaO are the active sites [44]. Peroxide ions in binuclear iron centers have also been proposed for the methane monooxygenase. Density function calculations by Siegbahn and Crabtree suggest that two iron ions in a binuclear complex become bridged by a peroxide bridge. These authors show that the Fe–O–O–Fe configuration is energetically more favorable than two single O bridges over the same Fe ion pair [45]. Therefore, an alternative rationalization for the formation of adsorbed nitro and nitrate groups could be the following sequence:

$$\left[HO–Fe^{2+}–\square–Fe^{3+}–OH\right]^{2+} + O_2 = \left[HO–Fe^{3+}–O–O–Fe^{3+}–OH\right]^{2+} \quad (6)$$

$$\left[HO–Fe^{3+}–O–O–Fe^{3+}–OH\right]^{2+} + 2NO = \left[HO–Fe–NO_2\ NO_2–Fe–OH\right] \quad (7)$$

$$[HO{-}Fe^{3+}{-}O{-}O{-}Fe^{3+}{-}OH]^{2+} + 2NO_2 = [HO{-}Fe{-}NO_3\,NO_3{-}Fe{-}OH]^{2+}. \quad (8)$$

### 4.4. Correlation between iron components and the catalytic activity

The ranking of the catalysts for the catalytic oxidation of NO to $NO_2$ follows exactly the same order as for the SCR of $NO_x$ with hydrocarbons [13]. For both reactions, Fe/MFI is the most active catalyst; it is followed by Fe,H/MFI, whereas the performances of Fe,Na/MFI and $Fe_2O_3$/HMFI are much inferior. This is in line with the reaction mechanism proposed by us for the SCR of $NO_x$ with hydrocarbons over Fe/MFI [33,46]. The first step is oxidation of NO to $NO_2$ and formation of an adsorbed nitro/nitrate complex, conventionally termed $NO_y$ ($y > 2$) on iron sites. These $NO_y$ complexes react with hydrocarbons forming N-containing adsorbates, which are able to react with $NO_2$, producing dinitrogen. The IR spectra in this study suggest that the oxidation of NO to $NO_2$ at room temperature will not be a rate-limiting step over Fe,Na/MFI or $Fe_2O_3$/HMFI. In fact, adsorbed $N_2O_3$ and $N_2O_4$ complexes appeared quickly upon exposing one of these samples to $NO + O_2$. However, the $NO_y$ bands were rather weak on both catalysts (Figs. 9 and 10). On the contrary, over Fe/MFI intensive $NO_y$ bands appear immediately, while formation of adsorbed $N_2O_3$ and $N_2O_4$ is slower (Fig. 8). These results illustrate that those sites where nitro and nitrate groups ($NO_y$) are formed are also responsible for the high NO oxidation activity. Obviously, dissociative desorption of nitro and nitrate groups will produce $NO_2$.

So the catalytic activity ranking reported in our previous work [13] over the four catalysts can be rationalized as follows.

$Fe_2O_3$/HMFI contains mainly small $Fe_2O_3$ particles at the external surface of the zeolite. They are not active for the adsorption of nitro and nitrate groups. As a result, this catalyst does not show high activity for the catalytic oxidation of NO to $NO_2$. It is therefore also a poor catalyst for the SCR of NO.

The features of $NO_x$ adsorption on ferric oxide nano-clusters inside zeolite channels are very similar to those of small $Fe_2O_3$ particles. It is therefore not surprising to see that Fe,Na/MFI, in which the nano-clusters are the major iron component, shows a catalytic performance similar to $Fe_2O_3$/MFI.

Over Fe/MFI at high metal loading obtained by the sublimation method, an oxygen-bridged binuclear iron complex might be present as part of the iron population of the zeolite. In addition small $Fe_2O_3$ particles, ferric oxide nano-clusters, and isolated iron ions will be present. This binuclear iron complex is highly active for the adsorption of nitro and nitrate groups, hence, it shows high catalytic activity. The slightly lower performance of Fe,H/MFI could be due to a smaller number of such binuclear iron sites.

It is also worth mentioning that the superior catalytic activity of Fe/MFI is not limited to the oxidation of NO to $NO_2$, and the selective reduction of $NO_x$ by hydrocarbons. In a previous paper, we showed that this catalyst is also quite active for the oxidation of hydrocarbons in an NO-free feed [13]. In this case, a large amount of partial oxidation products is formed. This is also easily rationalized in terms of the binuclear complex model: These centers are separated from each other and each has only one easily removable oxygen atom. Once this oxygen atom is consumed by reacting with the hydrocarbon molecule, chances are high that the partial oxidation product will be desorbed rather than reacting further on a different site. This situation is different from that on small $Fe_2O_3$ particles or nano-clusters, where a partial oxidation product can easily react further with other oxygen atoms, reaching a state of lower Gibbs free energy.

## 5. Conclusions

Small $Fe_2O_3$ particles, electron-deficient ferric oxide nano-clusters, isolated iron ions, and possibly oxygen-bridged iron binuclear complexes coexist over Fe/MFI catalysts. Their relative concentrations depend on the sample preparation method. Neither small $Fe_2O_3$ particles nor ferric oxide nano-clusters can strongly adsorb NO or $NO_2$. Binuclear iron oxo-ions are believed to be the active centers for the oxidation of NO to $NO_2$, but also for the formation

of $NO_y$ groups. Superoxide and/or peroxide ions are likely involved in the NO oxidation step. Fe/MFI prepared by sublimation with a high iron loading may contain more iron ions in the state of such binuclear iron oxo-ions. As a result, this catalyst shows high activity and selectivity for the oxidation of NO to $NO_2$ and for the SCR of $NO_x$ by hydrocarbons.

## Acknowledgements

This work was supported by the EMSI program of the National Science Foundation and the US Department of Energy Office of Science (CHE-9810378) at the Northwestern University Institute for Environmental Catalysis. Financial aid from the Director of the Chemistry Division, Basic Energy Sciences, US Department of Energy, Grant DE-FGO2-87ER13654, is gratefully acknowledged. We thank the DuPont-Northwestern-Dow Collaborative Access Team (DND-CAT) of the Synchrotron Research Center located at Sector 5 of the Advanced Photon Source in Argonne, IL, for their kind permission and help in collecting X-ray absorption spectroscopy data.

## References

[1] G.I. Panov, A.K. Uriarte, M.A. Rodkin, V.I. Sobolev, Catal. Today 41 (1998) 365.
[2] X. Feng, W.K. Hall, J. Catal. 166 (1997) 368.
[3] H.-Y. Chen, W.M.H. Sachtler, Catal. Today 42 (1998) 73.
[4] G.I. Panov, V.I. Sobolev, K.A. Dubkov, V.N. Parmon, N.S. Ovanesyan, A.E. Shilov, A.A. Shteinman, React. Kinet. Catal. Lett. 61 (1997) 251.
[5] V. Sobolev, G. Panov, A. Kharitonov, V. Romannikov, A. Volodin, K. Ione, J. Catal. 139 (1993) 435.
[6] N.S. Ovanesyan, A.A. Shteinman, K.A. Dubkov, V.I. Sobolev, G.I. Panov, Kinet. Catal. 39 (1998) 792.
[7] W.K. Hall, X. Feng, J. Dumesic, R. Watwe, Catal. Lett. 52 (1998) 13.
[8] T.V. Voskoboinikov, H.-Y. Chen, W.M.H. Sachtler, Appl. Catal., B 19 (1998) 279.
[9] K. Lázár, A.N. Kotasthane, P. Fejes, Catal. Lett. 57 (1999) 171.
[10] A.V. Kucherov, C.N. Montreuil, T.N. Kucherova, M. Shelef, Catal. Lett. 56 (1998) 173.
[11] H.-T. Lee, H.-K. Rhee, Catal. Lett. 61 (1999) 71.
[12] R. Joyner, M. Stockenhuber, J. Phys. Chem. B 103 (1999) 5963.
[13] H.-Y. Chen, X. Wang, W.M.H. Sachtler, Phys. Chem. Chem. Phys., submitted.
[14] H.-Y. Chen, W.M.H. Sachtler, Catal. Lett. 50 (1998) 125.
[15] B. Wichterlová, S. Beran, S. Bednářová, K. Nedomová, L. Dudíková, P. Jírů, Stud. Surf. Sci. Catal. 37 (1988) 199.
[16] S. Bordiga, R. Buzzoni, F. Geobaldo, C. Lamberti, E. Giamello, A. Zecchina, G. Leofanti, G. Petrini, G. Tozzola, G. Vlaic, J. Catal. 158 (1996) 486.
[17] J. Zhao, F.E. Huggins, Z. Feng, F. Lu, N. Shah, G.P. Huffman, J. Catal. 143 (1993) 499.
[18] El-M. El-Malki, R.A. van Santen, W.M.H. Sachtler, J. Phys. Chem. B 103 (1999) 4611.
[19] A. Brückner, R. Lück, W. Wieber, B. Fahlke, H. Mehner, Zeolites 12 (1992) 380.
[20] L.N. Mulay, N.L. Hoffman, Inorg. Nucl. Chem. Lett. 2 (1966) 189.
[21] A.F. Reid, H.K. Perkins, M.J. Sienko, Inorg. Chem. 7 (1968) 119.
[22] M. Chatterjee, D. Bhattacharya, N. Venkatathri, S. Sivasanker, Catal. Lett. 35 (1995) 313.
[23] G. Busca, V. Lorenzelli, J. Catal. 72 (1981) 303.
[24] S. Yuen, Y. Chen, J.E. Kubsh, J.A. Dumesic, N. Topsøe, H. Topsøe, J. Phys. Chem. 86 (1982) 3022.
[25] K.-I. Segawa, Y. Chen, J.E. Kubsh, W.N. Delgass, J.A. Dumesic, W.K. Hall, J. Catal. 76 (1982) 112.
[26] L.M. Aparicio, W.K. Hall, S.-M. Fang, M.A. Ulla, W.S. Millman, J.A. Dumesic, J. Catal. 108 (1987) 233.
[27] M.D. Amiridis, F. Puglisi, J.A. Dumesic, W.S. Millman, N.Y. Topsøe, J. Catal. 142 (1993) 572.
[28] L.J. Lobree, I.-C. Hwang, J.A. Reimer, A.T. Bell, J. Catal. 186 (1999) 242.
[29] L.J. Lobree, I.-C. Hwang, J.A. Reimer, A.T. Bell, Catal. Lett. 63 (1999) 233.
[30] K. Hadjiivanov, H. Knözinger, B. Tsynstsarski, L. Dimitrov, Catal. Lett. 62 (1999) 35.
[31] K. Hadjiivanov, J. Saussey, J.L. Freysz, J.C. Lavalley, Catal. Lett. 52 (1998) 103.
[32] J. Szanyi, M.T. Paffett, J. Catal. 164 (1996) 232.
[33] H.-Y. Chen, T. Voskoboinikov, W.M.H. Sachtler, J. Catal. 180 (1998) 171.
[34] Gmelin, Handbuch der Anorganischen Chemie vol. 4 Verlag Chemie, Berlin, 1936, p. 781.
[35] P. Marturano, L. Drozdová, A. Kogelbauer, R. Prins, J. Catal., submitted.
[36] B.J. Waller, J.D. Lipscomb, Chem. Rev. 96 (1996) 2625.
[37] A.G. Rosenzweig, C.A. Frederich, S.J. Lippard, P. Nordlund, Nature 366 (1993) 537.
[38] G.D. Lei, B.J. Adelman, J. Sárkány, W.M.H. Sachtler, Appl. Catal., B 5 (1995) 245.
[39] J. Sárkány, W.M.H. Sachtler, Stud. Surf. Sci. Catal. 94 (1995) 649.
[40] J. Sárkány, J. Mol. Struct. 410 (1997) 95.
[41] C.H. Rochester, S.A. Topham, J. Chem. Soc., Faraday Trans. I 75 (1979) 1259.

[42] B. Wichterlová, J. Dedecek, Z. Sobalik, in: M.M.J. Treacy, B.K. Marcus, M.E. Bisher, J.B. Higgins (Eds.), Proceedings of the 12th International Zeolite Conference, Materials Research Society, Baltimore, MD, 1998, p. 941.
[43] C.M. Fu, M. Deeba, W.K. Hall, Ind. Eng. Chem. Prod. R&D 19 (1980) 299.
[44] G. Mestl, M.P. Rosynek, J.H. Lunsford, J. Phys. Chem. B 101 (1997) 9329.
[45] P.E.M. Siegbahn, R.H. Crabtree, J. Am. Chem. Soc. 119 (1997) 3103.
[46] H.-Y. Chen, X. Wang, W.M.H. Sachtler, Appl. Catal. A, in press.